Springer

Dear Author,

Here are the proofs of your article.

- You can submit your corrections **online**, via **e-mail** or by **fax**.
- For **online** submission please insert your corrections in the online correction form. Always indicate the line number to which the correction refers.
- You can also insert your corrections in the proof PDF and **email** the annotated PDF.
- For fax submission, please ensure that your corrections are clearly legible. Use a fine black pen and write the correction in the margin, not too close to the edge of the page.
- Remember to note the **journal title**, **article number**, and **your name** when sending your response via e-mail or fax.
- **Check** the metadata sheet to make sure that the header information, especially author names and the corresponding affiliations are correctly shown.
- **Check** the questions that may have arisen during copy editing and insert your answers/ corrections.
- **Check** that the text is complete and that all figures, tables and their legends are included. Also check the accuracy of special characters, equations, and electronic supplementary material if applicable. If necessary refer to the *Edited manuscript*.
- The publication of inaccurate data such as dosages and units can have serious consequences. Please take particular care that all such details are correct.
- Please **do not** make changes that involve only matters of style. We have generally introduced forms that follow the journal's style.
  Substantial changes in content, e.g., new results, corrected values, title and authorship are not allowed without the approval of the responsible editor. In such a case, please contact the Editorial Office and return his/her consent together with the proof.
- If we do not receive your corrections **within 48 hours**, we will send you a reminder.
- Your article will be published **Online First** approximately one week after receipt of your corrected proofs. This is the **official first publication** citable with the DOI. **Further changes are, therefore, not possible.**
- The **printed version** will follow in a forthcoming issue.

Please note

After online publication, subscribers (personal/institutional) to this journal will have access to the complete article via the DOI using the URL: http://dx.doi.org/[DOI].
If you would like to know when your article has been published online, take advantage of our free alert service. For registration and further information go to: http://www.springerlink.com.

Due to the electronic nature of the procedure, the manuscript and the original figures will only be returned to you on special request. When you return your corrections, please inform us if you would like to have these documents returned.

Metadata of the article that will be visualized in OnlineFirst

Please note: Images will appear in color online but will be printed in black and white.		
ArticleTitle	Enhanced degradation of persistent pharmaceuticals found in wastewater treatment effluents using TiO_2 nanobelt photocatalysts	
Article Sub-Title		
Article CopyRight	Springer Science+Business Media Dordrecht (This will be the copyright line in the final PDF)	
Journal Name	Journal of Nanoparticle Research	
Corresponding Author	Family Name	**Hu**
	Particle	
	Given Name	**Anming**
	Suffix	
	Division	Centre for Advanced Materials Joining, Department of Mechanical and Mechatronics Engineering
	Organization	University of Waterloo
	Address	200 University Avenue West, N2L 3G1, Waterloo, ON, Canada
	Division	Waterloo Institute for Nanotechnology
	Organization	University of Waterloo
	Address	200 University Avenue West, N2L 3G1, Waterloo, ON, Canada
	Email	a2hu@uwaterloo.ca
Author	Family Name	**Liang**
	Particle	
	Given Name	**Robert**
	Suffix	
	Division	Centre for Advanced Materials Joining, Department of Mechanical and Mechatronics Engineering
	Organization	University of Waterloo
	Address	200 University Avenue West, N2L 3G1, Waterloo, ON, Canada
	Division	Waterloo Institute for Nanotechnology
	Organization	University of Waterloo
	Address	200 University Avenue West, N2L 3G1, Waterloo, ON, Canada
	Email	
Author	Family Name	**Li**
	Particle	
	Given Name	**Wenjuan**
	Suffix	
	Division	Centre for Advanced Materials Joining, Department of Mechanical and Mechatronics Engineering
	Organization	University of Waterloo
	Address	200 University Avenue West, N2L 3G1, Waterloo, ON, Canada
	Email	
Author	Family Name	**Zhou**
	Particle	
	Given Name	**Y. Norman**

	Suffix	
	Division	Centre for Advanced Materials Joining, Department of Mechanical and Mechatronics Engineering
	Organization	University of Waterloo
	Address	200 University Avenue West, N2L 3G1, Waterloo, ON, Canada
	Division	Waterloo Institute for Nanotechnology
	Organization	University of Waterloo
	Address	200 University Avenue West, N2L 3G1, Waterloo, ON, Canada
	Email	

Schedule	Received	19 July 2013
	Revised	
	Accepted	2 September 2013

Abstract	Pharmaceuticals in wastewater effluents are a current and emerging global problem and the development of cost-effective methods to facilitate their removal is needed to mitigate this issue. Advanced oxidation processes (AOPs), in particular UV/TiO_2, have potential for wastewater treatment. In this study, TiO_2 anatase phase nanobelts (30–100 nm in width and 10 μm in length) have been synthesized using a high temperature hydrothermal method as a means to photocatalyze the oxidation of pharmaceutical contaminants. We have investigated a model dye (malachite green), three pharmaceuticals and personal care products—naproxen, carbamazepine, and theophylline—that are difficult to oxidize without AOP processes. TiO_2 nanobelts were exposed to 365 nm UV illumination and the measured photocatalytic degradation rates and adsorption parameters of pharmaceuticals were explored using kinetic models. Furthermore we have determined the degree of pharmaceutical degradation as a function of solution pH, illumination time, temperature, and concentration of contaminant. In addition, the roles of active oxygen species—hydroxyl radial ($OH^{\cdot}$), positive holes (h^+), and hydrogen peroxide (H_2O_2)—involved were also investigated in the degradation process. These studies offer additional applications of hierarchical TiO_2 nanobelt membranes, including those harnessing sunlight for water treatment.

Keywords (separated by '-')	TiO_2 nanobelts - Photocatalysis - Surface adsorption - Pharmaceuticals - Sustainable development - EHS
Footnote Information	**Electronic supplementary material** The online version of this article (doi:10.1007/s11051-013-1990-x) contains supplementary material, which is available to authorized users.

Metadata of the article that will be visualized in OnlineAlone

Electronic supplementary material	Below is the link to the electronic supplementary material.Supplementary material 1 (PDF 58 kb)

J Nanopart Res (2013) 15:1990
DOI 10.1007/s11051-013-1990-x

RESEARCH PAPER

Enhanced degradation of persistent pharmaceuticals found in wastewater treatment effluents using TiO_2 nanobelt photocatalysts

Robert Liang · Anming Hu · Wenjuan Li · Y. Norman Zhou

Received: 19 July 2013 / Accepted: 2 September 2013

Abstract Pharmaceuticals in wastewater effluents are a current and emerging global problem and the development of cost-effective methods to facilitate their removal is needed to mitigate this issue. Advanced oxidation processes (AOPs), in particular UV/TiO_2, have potential for wastewater treatment. In this study, TiO_2 anatase phase nanobelts (30–100 nm in width and 10 μm in length) have been synthesized using a high temperature hydrothermal method as a means to photocatalyze the oxidation of pharmaceutical contaminants. We have investigated a model dye (malachite green), three pharmaceuticals and personal care products—naproxen, carbamazepine, and theophylline—that are difficult to oxidize without AOP processes. TiO_2 nanobelts were exposed to 365 nm UV illumination and the measured photocatalytic degradation rates and adsorption parameters of pharmaceuticals were explored using kinetic models. Furthermore we have determined the degree of pharmaceutical degradation as a function of solution pH, illumination time, temperature, and concentration of contaminant. In addition, the roles of active oxygen species—hydroxyl radial (OH·), positive holes (h^+), and hydrogen peroxide (H_2O_2)—involved were also investigated in the degradation process. These studies offer additional applications of hierarchical TiO_2 nanobelt membranes, including those harnessing sunlight for water treatment.

Keywords TiO_2 nanobelts · Photocatalysis · Surface adsorption · Pharmaceuticals · Sustainable development · EHS

Introduction

There are roughly 3.8 billion human beings that have limited or no access to a potable water source and about millions have succumbed to waterborne diseases each year (Malato et al. 2009). With the growing demand for clean water sources due to economic disparity, rapid urbanization, industrialization, and population growth, there is growing concern on the availability and strategies necessary to deliver potable water (Malato et al. 2009; Richardson 2008; Sua'rez et al. 2008; Wintgens et al. 2008). To exacerbate the situation, there are also emerging pollutants in

Electronic supplementary material The online version of this article (doi:10.1007/s11051-013-1990-x) contains supplementary material, which is available to authorized users.

R. Liang · A. Hu · W. Li · Y. N. Zhou
Centre for Advanced Materials Joining, Department of Mechanical and Mechatronics Engineering, University of Waterloo, 200 University Avenue West, Waterloo, ON N2L 3G1, Canada

R. Liang · A. Hu (✉) · Y. N. Zhou
Waterloo Institute for Nanotechnology, University of Waterloo, 200 University Avenue West, Waterloo, ON N2L 3G1, Canada
e-mail: a2hu@uwaterloo.ca

Journal : Medium 11051 | Dispatch : 12-9-2013 | Pages : 13
Article No. : 1990 | ☐ LE | ☐ TYPESET
MS Code : NANO-D-13-01222 | ✔ CP | ✔ DISK

wastewater effluents that have potential adverse health effects; these include, but are not limited to, textile dyes, pharmaceuticals, steroid estrogens, personal care products, plasticizers, and algal toxins (Bousselmi et al. 2004; Malato et al. 2009; Mozia et al. 2007; Naddeo et al. 2011; Rizzo et al. 2009). Addressing current and future problems require new robust methods and technologies of purifying water at lower cost, energy, and environmental impact than current methods.

Over the past few decades, advanced oxidation processes (AOPs) have been given attention as effective technologies for remediation and removal of persistent pollutants in water and wastewater (Bloecher 2007; Sirés and Brillas 2012). AOPs are aimed to convert organic pollutants, and their constituents, into inorganic molecules that are, for the most part, harmless. To elaborate, AOPs generate hydroxyl radicals (HO·), a powerful and very reactive oxidant that can attack almost all organic compounds. In addition, HO· radicals react 10^6–10^{12} times more rapidly than alternative oxidants such as ozone (O_3), and have a high redox potential (2.80 V vs. normal hydrogen electrode, NHE), second to fluorine, which is highly toxic, in Table 1 (Naddeo et al. 2011; Pignatello et al. 2006; Solarchem Environmental Systems 1994). There are several AOP processes currently used such as ozonation (O_3), hydrogen peroxide (H_2O_2), TiO_2, and Fenton (Fe^{2+}) processes. All these processes may be improved using ultraviolet (UV) irradiation and ultrasonication (Naddeo et al. 2011).

Of particular interest to our group are TiO_2–UV processes. TiO_2 is a photocatalyst that when illuminated with light radiation, the photons get absorbed, provided that the energy meets the condition $h\nu \geq E_g$ (band-gap energy), generate enough energy to move electrons from the valence band to the conduction band, and simultaneously, holes (vacancies left by electrons) are created in the valence band (Fujishima et al. 2000; Malato et al. 2009). These electron/hole pairs either they recombine, and produce thermal energy, or migrate to the photocatalyst surface where they participate in redox reactions with adsorbed substances on the TiO_2 liquid/solid interface (Quiroz et al. 2011). These photogenerated holes and electrons have a redox potential around +2.53 and −0.52 V, respectively, in pH 7 studied under TiO_2 photoanode, Pt cathode, and a reference standard hydrogen electrode (SHE) (Solarchem Environmental Systems 1994). TiO_2 nanoparticles have successfully been applied to prototype wastewater treatment plants (WWTPs) and research has been conducted using TiO_2 slurries and immobilized membranes (Albu et al. 2007; Bousselmi et al. 2004; Hu et al. 2011; Malato et al. 2002; Zhang et al. 2009). TiO_2 slurries have higher photocatalytic degradation rates than immobilized membranes, however, they require an extra cost intensive separation step to recover the suspended TiO_2 (Hu et al. 2011; Naddeo et al. 2011). Although conventional TiO_2 nanoparticles are effective in their removal of organic compounds, they suffer from the propensity of electron and hole recombination; however, TiO_2 nanowires and hierarchical structures have been shown to reduce recombination and increase photocatalytic efficiency (Wu et al. 2013; Yang et al. 2009; Zheng et al. 2010).

Personal care products and pharmaceuticals (PPCPs) are a group of emerging pollutants that are being released into the environment, without having been regulated either due to lack of information regarding their occurrence and environmental effects (Hu et al. 2013; Naddeo et al. 2011). These pharmaceuticals vary in their removability in wastewater treatment effluents. Conventional drinking water treatments, such as coagulation/flocculation, filtration, and sedimentation, have been largely ineffective against treating pharmaceuticals below detection limits. Ozone oxidation, a capital intensive treatment option, has become part of WWTPs (Klavarioti et al. 2009; Rizzo et al. 2009; Rosal et al. 2010) to address this concern. As shown in Table 1, O_3 has a lower positive redox potential than HO·. In addition, under other AOP processes such as UV–C illumination ($\lambda \leq 254$ nm), PPCP compounds such as naproxen,

Table 1 A list of oxidants and their redox potentials with respect to normal hydrogen electrode

Oxidant	Redox potential (V vs. NHE, 25 °C)
F_2	+3.03
HO·	+2.80
O·	+2.42
O_3	+2.07
H_2O_2	+1.78
HO_2·	+1.70
Cl_2	+1.36

Journal : Medium 11051 Dispatch : 12-9-2013 Pages : 13
Article No. : 1990 LE TYPESET
MS Code : NANO-D-13-01222 CP DISK

carbamazepine, and theophylline degrade very slowly and require UV illumination of less than 200 nm to initiate photolysis (Giri et al. 2010; Kim and Tanaka 2009). As shown in this work, these PPCPs can be degraded faster using heterogeneous photocatalysis, under longer UV wavelengths.

In this study, we have used a facile method of fabricating TiO_2 nanowires as reported in our previous studies (Hu et al. 2011, 2013), in order to perform a series of tests on known persistent PPCPs and evaluate the photocatalytic degradation rates of their parent compounds as a proof-of-concept. High concentrations of PPCPs, compared to those found in wastewater effluents, were used because of detector limitations. Some of these PPCPs are produced from industry, agriculture, and consumer goods, while others are unintentionally formed by-products from industrial processes (Richardson et al. 1996; Selcuk 2010). We performed a series of experiments to demonstrate the photocatalytic degradation of a model dye (malachite green) and select pharmaceuticals, including naproxen, carbamazepine, and theophylline. Theophylline, in particular, was chosen to conduct temperature, pH, and concentration dependence studies because of its high solubility in water compared to the other two compounds and fewer studies conducted on its photocatalytic degradation.

Experimental procedures

TiO_2 nanobelt synthesis

TiO_2 nanobelts were synthesized using a method developed in a previous study (Hu et al. 2011). In a 125 mL Teflon-lined stainless steel autoclave (Parr Instruments), $Na_2Ti_3O_7$ nanobelts were grown for 72 h in 60 mL NaOH (10 M) alkaline solution at 190 °C using 2 g of P25 Aeroxide™ (Evonik Industries AG) as the TiO_2 source. After cooling the reactor, the suspended nanobelts were transferred into 50 mL conical tubes and centrifuged five times using Millipore water. Subsequently, the sodium titanate ($Na_2Ti_3O_7$) nanobelts were transferred into a beaker in 0.1 M HCl solution, and through an ion exchange process hydrogen titanate ($H_2Ti_3O_7$) is obtained. Afterward, $H_2Ti_3O_7$ was dried in a furnace for 80 °C for 8 h to obtain a powder. The fabricated nanobelts were annealed at 700 °C for 1 h to form TiO_2 nanobelts.

Material characterization

The phase and microstructure of fabricated TiO_2 nanowires were examined by X-ray diffraction, Raman spectroscopy, Scanning electron microscopy (SEM), and High-resolution transmission electron microscopy (HRTEM). Powder XRD measurements were performed on a Rigaku SA-HF3 X-ray diffractometer using Cu Kα radiation (1.54 Å) X-ray source equipped with an 800 μm collimator, operating at an excitation voltage of 50 kV. The obtained diffraction patterns were collected from 10^o to 90^o at a scanning rate of 1.5^o per minute. Raman spectroscopy was conducted using a Raman microscope (Renishaw inVia microscope equipped with 488 nm Ar ion laser). The morphology of the as-synthesized TiO_2 nanobelts was evaluated using a ZEISS LEO 1550 FE-SEM at an accelerating voltage of 10 kV. HRTEM observation was conducted using a JEOL 2010F at the Canadian Centre for Electron Microscopy (Hamilton, Ontario, Canada). The TEM samples were prepared by suspending TiO_2 nanobelts in ethanol and drip casting the solution onto lacey carbon grids. The images were processed using Gatan Microscopy Suite: Digital Micrograph™ (Ver. 2.11.1404.0). The specific surface area was determined using Brunauer–Emmett–Teller (BET) surface analyzer (Quantachrome Instruments NOVA 2200) using N_2 adsorption data. The bandgap of TiO_2 nanobelts was determined by recording the diffuse reflectance spectra using a Shimdazu UV-2501PC UV–Vis-NIR spectrophotometer equipped with an integrating sphere accessory, with $BaSO_4$ as reference scatter.

Adsorption and photocatalytic degradation

Surface adsorption experiments were carried out by dispersing 40 mg of TiO_2 nanomaterial into a slurry in a Pyrex beaker containing 200 mL of malachite green dye, naproxen, carbamazpine, and theophylline (from Sigma-Aldrich) solutions of varying concentrations in the dark, at room temperature, with adsorption accelerated by magnetic stirring for 90 min. In particular, the poor water-soluble drugs, naproxen and carbamazepine, were studied under their maximum aqueous solubility limits of 60.1 ± 2 and 125.0 ± 2 mg L^{-1}, respectively (Maoz and Chefetz 2010).

Photocatalytic degradation was assessed with the same conditions as surface adsorption experiments,

Journal : Medium 11051 Dispatch : 12-9-2013 Pages : 13
Article No. : 1990 LE TYPESET
MS Code : NANO-D-13-01222 CP DISK

but in the presence of UV illumination using a 100 W middle pressure mercury lamp (UVP, Blak-Ray® Model B 100AP) at a maximum peak emission wavelength at 365 nm. The distance between the UV lamp surface (quartz) and surface of the water matrix was 5 cm, the minimum distance to fit the Pyrex beaker under the UV lamp, with an intensity of 2.1 mW cm^{-2}. To saturate the surface sites of the nanomaterials before photocatalytic degradation, each solution was first stirred in the dark for at least 30 min. Subsequently, the UV lamp was turn on and the photocatalytic degradation experiment was conducted for 90 min. In order to determine the active radical species in the TiO_2-pharmaceutical solution, potassium iodide (KI) and isopropanol (*i*-PrOH) were used as selective free radical scavengers during degradation. The concentrations of KI and *i*-PrOH in the initial reaction solution were both 1 mM, which were described in a previous study (Zhang et al. 2008).

All samples were centrifuged at 3,200 rpm for 30 min, after the aforementioned experiments, to remove TiO_2 from the water matrix for analysis. A UV–Vis–Near IR spectrometer (Shimadzu UV-2501PC) was used to analyze these compounds from a spectral range of 200–800 nm, with a detector path length of 10 cm. The experiments were reproducible with errors less than 5 % (3 trials). Serial dilutions of standards were used to determine integrated peak areas of each standard and create calibration curves, which were employed to establish concentrations for samples. Data analysis was conducted on the UV Probe (Shimadzu Corporation, ver. 2.10).

Kinetic modeling

Adsorption model

A pseudo-second-order rate equation was used to evaluate the adsorption mechanism and is given by Eqs. 1 and 2 (Sun and Yang 2003):

$$\frac{t}{q_t} = \frac{1}{kq_e^2} + \frac{1}{q_e}t \quad (1)$$

$$q_t = \frac{(C_o - C_t)}{C_o} \quad (2)$$

where q_t and q_e (g/g) are adsorption capacities at time t (min) and at equilibrium, respectively, k is the initial adsorption rate constant, C_o is the initial concentration, and C_t is the concentration at time t. The values of k and q_e are obtained from the linear plot of $\frac{t}{q_t}$ versus t, and if the fit of the data is linear, it suggests that chemisorption takes places (Ho and McKey 1998; Kumar et al. 2005).

Intraparticle diffusion model

The Weber-Morris Model was used to evaluate intra-particle diffusion from mass transfer processes and is given by Eq. 3 (Weber and Morriss 1963):

$$q_t = k_i t^{\frac{1}{2}} + c \quad (3)$$

where k_i is the intra-particle diffusion rate constant and c is a constant. The intra-particle diffusion rate, k_i, may be separated into diffusion stages based on macro-, meso-, and micro-pore-structures of the adsorbent (Allen et al. 1989; Walker et al. 2003). Plotting q_t versus $t^{1/2}$ gives two linear sections of the curve demonstrating a transition from macro-pore diffusion to micro-pore diffusion. The slopes of the two diffusion regions give the intra-particle diffusion rate for that region.

Photocatalytic degradation model

The photocatalytic degradation can be described using a pseudo first-order kinetic model (Eq. 4) and its integrated form (Eq. 5):

$$-\frac{dC}{dt} = k_{ap}C \quad (4)$$

$$\ln(C/C_o) = k_{ap}t \quad (5)$$

where C_o is the initial concentration, C is a concentration, k_{ap} is the apparent rate constant, and t is time. A $\ln\left(\frac{C}{C_o}\right)$ versus t plot and a line of best fit yields k_{ap}.

Results and discussion

Material analysis

Figure 1 shows XRD patterns of TiO_2 nanobelts and P25 Aeroxide™. There are several characteristic anatase diffraction peaks that are seen in both samples, which come from (101), (004), (200), (105), (211), (204), (116), (220), and (215) planes. However, P25

Journal : Medium 11051 Dispatch : 12-9-2013 Pages : 13
Article No. : 1990 LE TYPESET
MS Code : NANO-D-13-01222 CP DISK

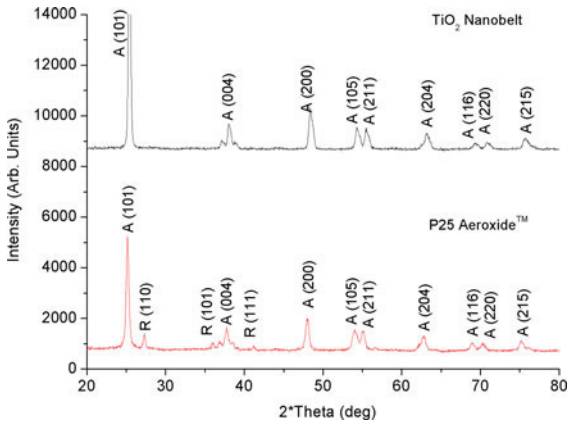

Fig. 1 X-ray diffraction patterns of synthesized TiO_2 nanobelts and P25 Degussa TiO_2 nanoparticles

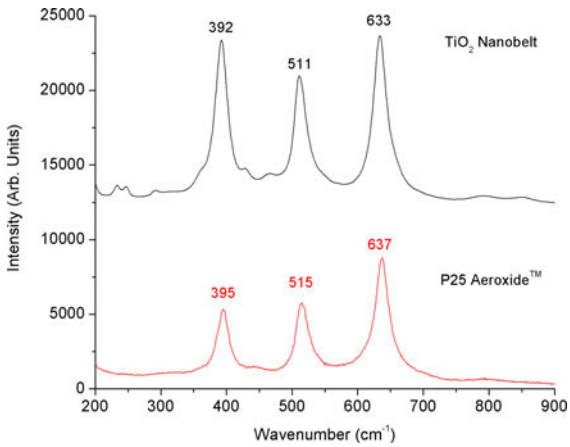

Fig. 2 Raman spectra of TiO_2 nanobelts and TiO_2 P25 Degussa using a laser excitation wavelength of 488 nm

Aeroxide™ does contain a minor amount of rutile, as seen in the XRD spectra, which indicate the presence of (110), (101), and (111) diffraction peaks of the rutile phase. The XRD results are reconfirmed by Raman spectra analysis in Fig. 2, which depicts TiO_2 nanobelts and P25 Aeroxide™. The typical Raman modes at 395, 515, and 637 cm^{-1} are clearly observed (Sikuvhihulu et al. 2008; Zárate et al. 2007), but the lower modes at 144 and 197 cm^{-1} are out of the detective range of the device. There is also a small peak at 247 cm^{-1} of the grown nanowires, which may possibly be due to a minor amount of amorphous TiO_2 (Li et al. 2010; Mazza et al. 2007).

The FESEM images (Fig. 3) depict hierarchical TiO_2 nanobelts with widths ranging from 30 to 100 nm and lengths in the range of tens of μm. This variation in the size distribution of the nanobelts is consistent with previous studies where alkaline media is used (Hu et al. 2011). In addition, the specific surface area of the nanobelts obtained is 21.52 $m^2\ g^{-1}$. It is also apparent that these hierarchical structures are not only composed of nanobelts, but also of nanoparticles and truncated rods fused on the nanobelt surface.

Using HRTEM, the detailed lattice structure of TiO_2 nanobelts is shown in Fig. 4. Figure 4a shows a single nanobelt where the indexed selected area electron diffraction (SAED) is obtained in the highlighted area using a zone axis of [001]. The indexed SAED pattern indicates that the crystal structure can be attributed to the anatase phase, which is a tetragonal structure, in agreement with XRD and Raman results. No $Na_2Ti_3O_7$ (monoclinic) is evident in HRTEM analysis. Furthermore, the growth direction of the nanobelts is in the {100} family of directions, which is consistent with another study (Li et al. 2008). Therefore, it is reasonable to conclude that anatase is the dominant composition of the nanobelts. Figure 4b reveals the crystal lattice structure of the anatase TiO_2 nanobelt and the dominant crystal planes in the observed nanobelts from the *d*-spacing of the lattice, which is 3.8 Å and corresponds to the <100> family of planes.

The bandgap of TiO_2 nanobelts was determined by using the Tauc method (Lin et al. 2006; Tauc et al. 1966; Yin et al. 2000; Wu et al. 2009). The diffuse reflectance spectrum was converted to a plot of $[h\nu F(R)]^{1/n}$ versus hν, where h is Planck's constant, ν is the frequency, R is the reflectance, n denotes the nature of the sample transition, and $F(R)$ is the Kubelka–Munk function (Lin et al. 2006), given by the equation:

$$F(R) = \frac{(1-R)^2}{2R}. \quad (6)$$

The value of the exponent n is $n = 2$ because TiO_2 is an indirect bandgap semiconductor. The bandgap was obtained by taking the intercept of the tangent at the inflection point (Fig. S1). The optical bandgap for TiO_2 nanobelts and P25 Aeroxide™ is 3.23 and 3.06 eV, respectively. The P25 has lower bandgap energy than TiO_2 nanobelts because it is a mixture of anatase and rutile phases, whereas TiO_2 nanobelts are predominantly anatase. The rutile phase has the lower bandgap energy than the anatase phase (Paola et al.

Journal : Medium 11051 Dispatch : 12-9-2013 Pages : 13
Article No. : 1990 LE TYPESET
MS Code : NANO-D-13-01222 CP DISK

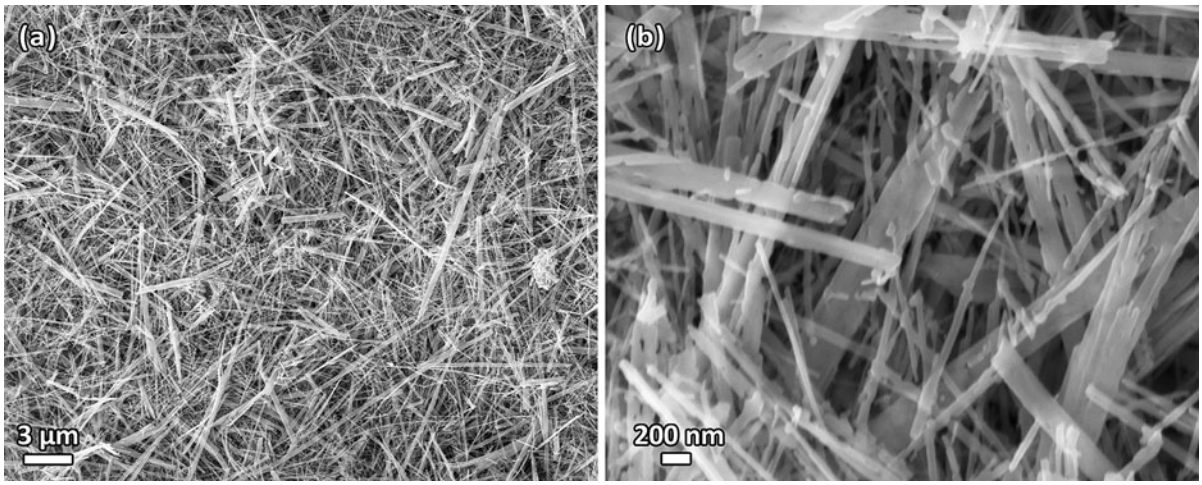

Fig. 3 FESEM of hierarchical TiO_2 nanobelts: **a** low magnification of TiO_2 nanobelts and **b** high magnification of TiO_2 nanobelts

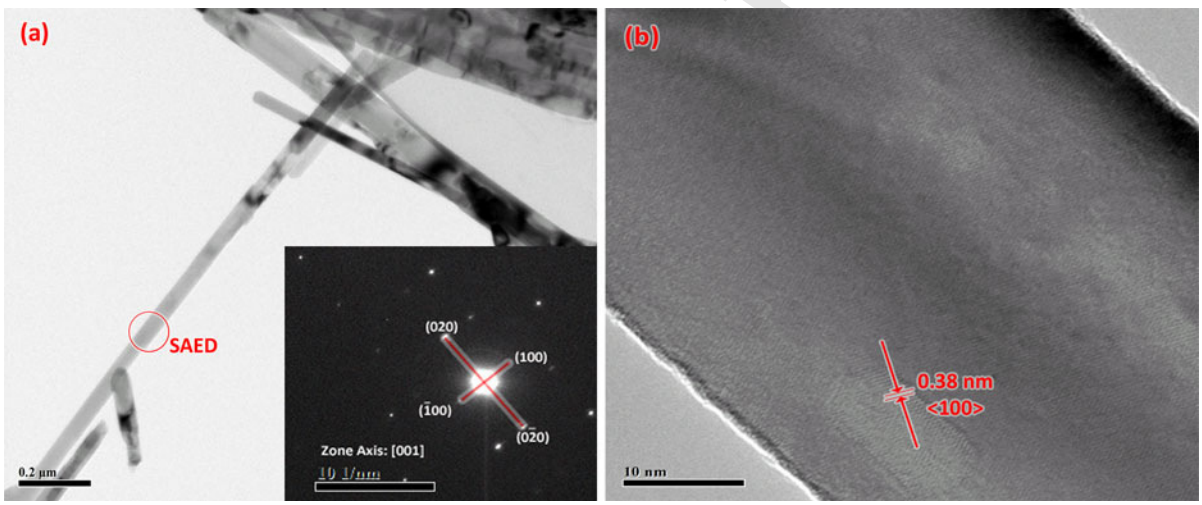

Fig. 4 HRTEM images of hierarchical TiO_2 nanobelts: **a** low magnification of single nanobelt with indexed SAED pattern and **b** high resolution of nanobelts with crystal *d*-spacing of 0.38 nm

2013). The high band-gap is of importance to yield strong oxidizing hydroxyl radicals through photocatalytic degradation (see Table 1), which can attack almost all aquatic organic contaminants.

Adsorption and photocatalytic degradation of malachite green

The adsorption and photocatalytic degradation kinetics of malachite green was conducted using TiO_2 nanobelts suspended in Millipore water as seen in Figs. 5 and 6. The adsorption capacity was saturated within the time frame of the experiment (Fig. 5b). From the pseudo-second-order model in Fig. 5a, the adsorption capacity of TiO_2 nanobelts is 74.34 mg g^{-1} and the initial sorption rate is 1.89×10^{-2} min^{-1}. From the Weber-Morris Plot (Fig. 5b), the intraparticle diffusion rate constants are given by $k_1 = 1.91 \times 10^{-2}$ min^{-1} and $k_2 = 1.19 \times 10^{-3}$ min^{-1}, which is roughly an order of magnitude less than k_1. The macro-pore diffusion constant, k_1, of adsorbing malachite green particles onto TiO_2 is quicker than the micro-pore diffusion constant, k_2, of adsorbing malachite green molecules because the macropore sites are accessible, whereas micropores

Journal : Medium 11051 Dispatch : 12-9-2013 Pages : 13
Article No. : 1990 LE TYPESET
MS Code : NANO-D-13-01222 CP DISK

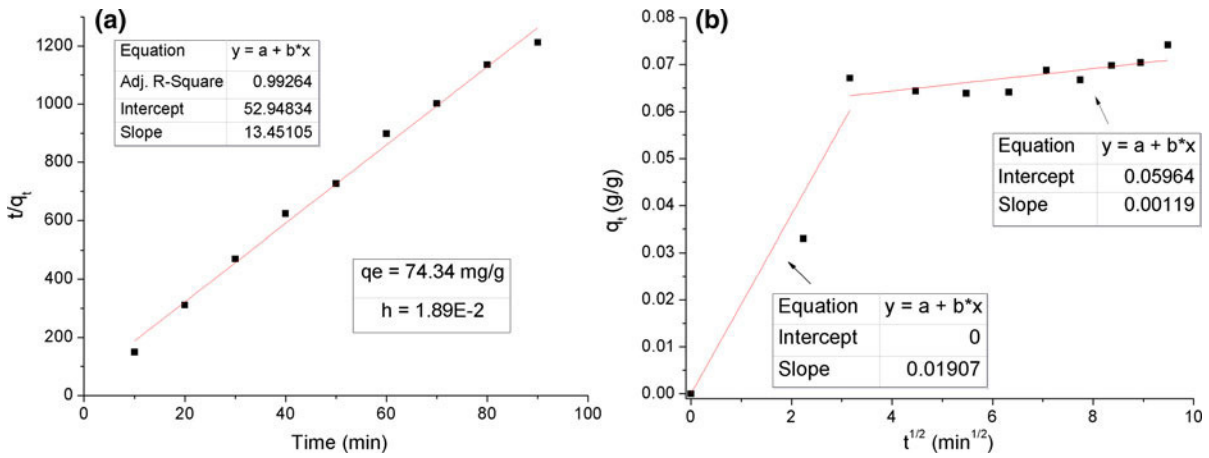

Fig. 5 Kinetic model of malachite green (initial concentration: 10 ppm) adsorption under dark conditions: **a** pseudo-second-order adsorption model of TiO_2 nanobelt adsorbent and **b** Weber-Morris plot of intraparticle diffusion

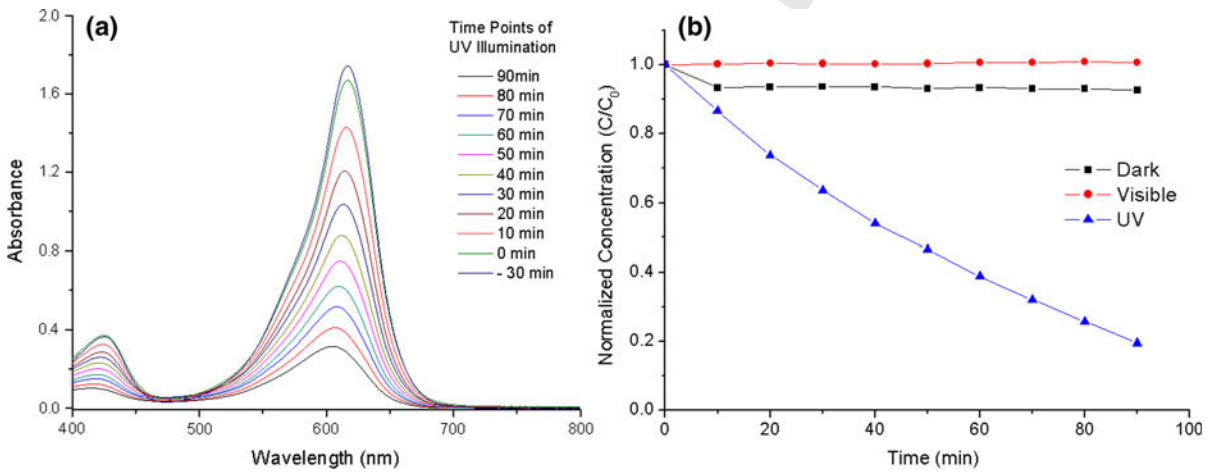

Fig. 6 Malachite green (initial concentration: 10 ppm) degradation with: **a** UV–Vis spectrum of malachite green at various time points before and after UV illumination and **b** normalized concentration versus time under dark, visible, and UV conditions

are the least accessible sites of adsorption and will take malachite green longer to interact with those sites.

Although, the BET surface area and adsorption capacity of the nanobelts are lower (21.52 $m^2\ g^{-1}$) than that of commercial P25 nanoparticles (50.69 $m^2\ g^{-1}$), a greater photocatalytic degradation rate than P25 as reported in our earlier study using TiO_2 nanowires and P25 to investigate the photocatalytic degradation of venlafaxine, fluoxetine, and sulfamethoxazole (Hu et al. 2013). The photocatalytic degradation is enhanced using TiO_2 nanobelts because it will reduce recombination when compared to P25 nanoparticles due to a decrease of grain boundary defects in one dimensional nanostructures (Wu et al. 2013; Zheng et al. 2010; Yang et al. 2009). Figure 6 indicates that the apparent photocatalytic degradation rate for malachite green is $1.67 \times 10^{-2}\ min^{-1}$ ($R^2 = 0.995$) under UV illumination (peak wavelength = 365 nm), however, no degradation is observed under visible light conditions (400–800 nm) due to a high optical bandgap of TiO_2 nanobelts (3.23 eV) and a low absorption of photons in that wavelength range. The 3.23 eV bandgap of TiO_2 nanobelts requires light radiation with a wavelength of 384 nm or lower to generate electron–hole pairs that participate in redox reactions.

Journal : Medium 11051 Dispatch : 12-9-2013 Pages : 13
Article No. : 1990 LE TYPESET
MS Code : NANO-D-13-01222 CP DISK

Table 2 Values obtained from pseudo-first-order, pseudo-second-order, and Weber-Morris models for dark adsorption and UV illumination of naproxen, theophylline, and carbamazepine

PPCP	Dark adsorption					UV illumination	
	Pseudo-second-order model			Weber-morris model		Pseudo-first-order model	
	Initial sorption rate (kq_e^2, min^{-1})	Equilibrium adsorption capacity (q_e, mg g^{-1})	R^2	Intraparticle diffusion rate constant 1 (k_1, min^{-1})	Intraparticle diffusion rate constant 2 (k_2, min^{-1})	Apparent photocatalytic degradation rate constant (k_{ap}, min^{-1})	R^2
Npx	1.56×10^{-1}	4.51	0.962	3.10×10^{-3}	-2.00×10^{-3}	6.16×10^{-2}	0.957
Thyp	7.58×10^{-2}	21.59	0.997	7.27×10^{-3}	-1.49×10^{-4}	9.12×10^{-2}	0.996
Cbp	3.66×10^{-2}	16.48	0.993	5.34×10^{-3}	-1.61×10^{-3}	2.91×10^{-2}	0.989

Npx Naproxen, *Thyp* Theophylline, *Cbp* Carbamazepine

Adsorption and photocatalytic degradation of selected pharmaceuticals

The adsorption and photocatalytic degradation of naproxen, theophylline, and carbamazepine were evaluated using kinetic models—pseudo-first-order, pseudo-second-order, and Weber-Morris—as shown in Table 2. The pharmaceuticals were subjected to adsorption and photocatalytic degradation experiments using an initial concentration of around 15 ppm at room temperature and pH 6.8. The adsorption for all pharmaceuticals follows a pseudo-second-order model and its intraparticle diffusion parameters' may be found using a Weber-Morris plot; whereas the photocatalytic degradation follows a pseudo-first-order model.

It is apparent that theophylline is easily degraded compared to naproxen and carbamazepine using a UV/TiO_2 process from their apparent photocatalytic degradation rate constants, k_{ap}, obtained from Fig. 7 and Table 2 (See Fig. S2 and Fig.S3 for calibration curves and UV–Vis spectra). This is possibly due to a greater adsorption capacity (21.59 mg g^{-1}) than naproxen (4.51 mg g^{-1}) and carbamazepine (16.48 mg g^{-1}). In addition, the macropore diffusion rate, k_1, of theophylline onto the surface of TiO_2 is much higher than the other two pharmaceuticals suggesting that theophylline molecules are able to occupy available surface sites on TiO_2 quicker than the other two pharmaceuticals, thereby allowing radicals to oxidize the molecule sooner. However, the negative values of the intraparticle rate constant, k_2, seem to suggest that desorption rate increases in theophylline, carbamazepine, and naproxen after a certain period of time, where all macropore sites are occupied by the pharmaceutical adsorbents.

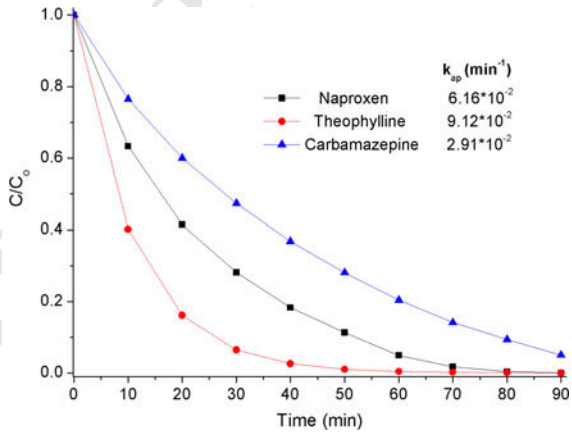

Fig. 7 Photocatalytic degradation of three pharmaceuticals (15 ppm): naproxen, theophylline, and carbamazepine

Giri et al. (2010) conducted a vast analysis of various AOP processes, including UV/TiO_2 anatase nanoparticles and UV/H_2O_2, with various pharmaceuticals at a concentration of 1 ppm. From their data, naproxen has a k_{ap} value of 6.23×10^{-2} min^{-1} and 7.51×10^{-2} min^{-1} under UV/TiO_2 nanoparticles and UV/H_2O_2, respectively. On the other hand, carbamazepine had a rate constant of 2.17×10^{-3} and 2.17×10^{-2} min^{-1} under UV/TiO_2 nanoparticles and UV/H_2O_2, respectively. These values are lower than our UV/TiO_2 nanobelts due to different nanostructures used, despite having an initial concentration in the order of magnitude less than the one reported here (15 ppm) and using a shorter wavelength UV source that is conducive to producing HO· radicals via photolysis.

Journal : Medium 11051 Dispatch : 12-9-2013 Pages : 13
Article No. : 1990 LE TYPESET
MS Code : NANO-D-13-01222 CP DISK

When comparing the theophylline degradation under UV/H_2O_2 and UV/TiO_2 nanobelts (Fig. S4), theophylline slowly degrades under 10 mM H_2O_2 with UV illumination ($k_{ap} = 3.65 \times 10^{-3}$ min^{-1}), whereas the degradation performance using TiO_2 with UV illumination is an order of magnitude greater ($k_{ap} = 5.68 \times 10^{-2}$ min^{-1}). In addition, theophylline degrades extremely slowly using only UV illumination at wavelengths of 365 and 254 nm as shown in Fig. S4 and is consistent with by Kim and Tanaka (2009).

Theophylline photocatalytic degradation parameters

Reaction oxygen species in theophylline

The reactive oxygen species has been studied previously in TiO_2 nanoparticles, where HO·, holes (h^+), and H_2O_2 are identified as dominant oxygen species (Maoz and Chefetz 2010; Zhang et al. 2008). Figure 8 indicates the photocatalytic degradation rates when potassium iodide and isopropanol quenchers were added to the TiO_2-theophylline slurry. Potassium iodide is used to scavenge valence band holes and hydroxyl radicals, whereas isopropanol is selective to hydroxyl radials (Zhang et al. 2008). From the photodegradation rates, the HO· contribution to the reaction was 75 % and the h^+ concentration was determined to be 20 %. The contribution of other reactive oxygen species, which include H_2O_2, HO_2 ·, and O_2^- is around 5 %. Surface hydroxyls scavenge valence holes to eventually produce HO·, which are the primary oxidizing species in photocatalytic reactions (Arrouvel et al. 2004; Cho et al. 2005; Henderson et al. 2003; Ishibashi et al. 2000). Although, theophylline's effect on the results (Lapenna et al. 1995) was mitigated by increasing the isopropanol concentration 1 mM, from 0.1 mM established in previous studies using different compounds (Sun and Yang 2003; Zhang et al. 2008).

Temperature effects

Photocatalytic systems generally do not require heating and are able to operate at room temperature. However, the apparent activation energy is often a small value at a certain temperature range (Lin et al. 2013). The apparent activation energy can be measured using the Arrhenius equation (Eq. 6):

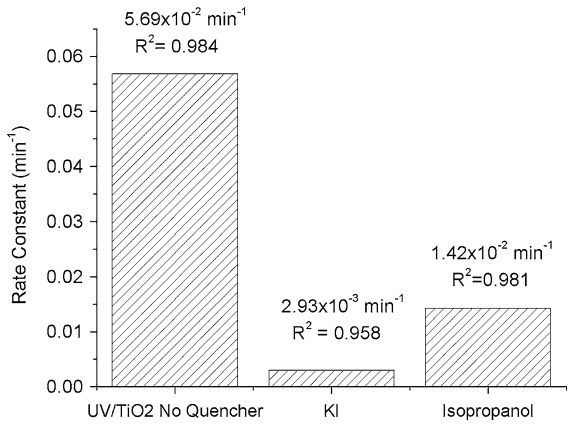

Fig. 8 Composition of reactive oxidative species determined using isopropanol (1 mM) and potassium iodide (1 mM) quenchers in the photocatalytic degradation of theophylline

$$k = Ae^{-\left(\frac{E_a}{k_b T}\right)} \quad (7)$$

where E_a is the apparent activation energy, k_b is the Boltzmann constant, k is the rate constant, A is the pre-exponential factor, and T is the temperature. The apparent activation energy, E_a, is obtained from the slope of the In (k) versus $1/T$ plot. The obtained apparent activation energy from the temperature range of 4–60 °C is 3.37 kJ mol^{-1}, which is similar to the dye compound degradation using Degussa P25 nanoparticles obtained in other studies (Barka et al. 2008; Bouzaida et al. 2004). The true activation energy depends on other parameters which include light flux and oxygen concentration (Barka et al. 2008).

As seen in Fig. 9, the photocatalytic degradation rate increases as a function of temperature at a range of 4–60 °C. In other words, the diffusion of theophylline onto the TiO_2 nanobelt surface is temperature dependent. Increasing the temperature increases the diffusion rate of theophylline onto TiO_2 nanobelt surface, and hence the photocatalytic degradation rate of the adsorbed pharmaceutical. An increase in temperature also helps the photocatalytic reaction to complete much more efficiently with electron–hole recombination (Barka et al. 2008).

pH effects

The pH of the TiO_{-2} suspension was altered by either adding dilute HCl or NaOH to acidify or alkalinize the solution. The pH of the TiO_2 slurry containing theophylline influences the surface ionization state of TiO_2:

Journal : Medium 11051 Dispatch : 12-9-2013 Pages : 13
Article No. : 1990 LE TYPESET
MS Code : NANO-D-13-01222 CP DISK

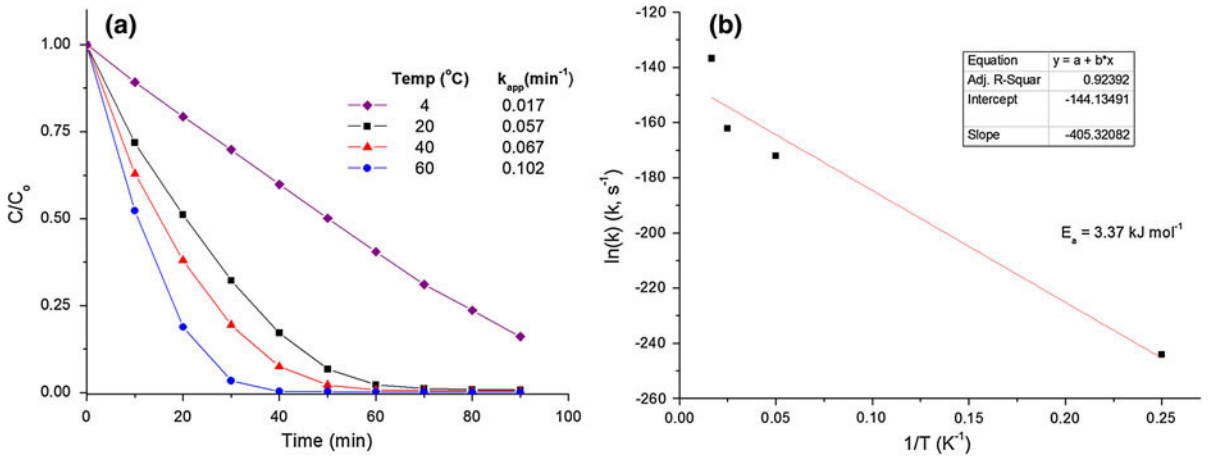

Fig. 9 Photocatalytic degradation of theophylline at temperatures of 4, 20, 40, and 60 °C. Activation energy from temperature range of 4–60 °C is 56.2 J mol^{-1}

$$TiOH + H^+ \leftrightarrow TiOH_2^+ \quad (8)$$

$$TiOH + OH^- \leftrightarrow TiO^- \quad (9)$$

because it is amphoteric in nature. The flatband potential of the TiO_2 nanobelt is a function of pH. When OH^- and H^+ ions are chemisorbed from aqueous solutions, at a certain pH value, the overall charge of the adsorbed ions will be at zero, or the isoelectric point (IEP). When the pH of the solution is close to the IEP of TiO_2, particles and other nanostructures tend to agglomerate due to the van der Waals attraction. The TiO_2 nanobelts have positive charges on the surface in neutral water, according to another study, where TiO_2 nanobelts were obtained in the same fashion and have a positive zeta potential of +9.65 mV at pH 7.0 (Zhou et al. 2010).

The pH is also influenced by the adsorption and desorption of the main reactants and intermediates of theophylline on the surface of TiO_2 because the increase in equilibrium adsorption capacities in Table 3 suggests that the pH increases adsorption of theophylline onto surface sites of TiO_2 (Al-Qaradawi and Salman 2004; He et al. 2005; Yao et al. 2004). The adsorption capacity of TiO_2 roughly increases fourfold from pH 4.0 (10.04 mg g^{-1}) to 10.0 (36.79 mg g^{-1}). Consequently, the apparent photocatalytic rate constants obtained in Table 3 indicate that the photocatalytic degradation increases with pH, and this observation has also been confirmed by other studies (Bahnemann et al. 1991; Houas et al. 2001; Rengifo-Herrera et al. 2011). Furthermore, the increase in photocatalytic degradation may also be partially attributed to alkaline solutions tending to favor HO· formation because they are formed between the reaction between OH, available from dissociated NaOH, and h^+. Consequently, HCl was used to acidify the TiO_2 solution, and the Cl^- ions from HCl are HO· scavengers, thereby reducing the degradation rate of theophylline.

Table 3 Pseudo-second-order model values—photocatalytic degradation of theophylline at pH values of 4.0, 6.8, and 10.0

pH	Dark adsorption			UV illumination	
	Pseudo-second-order model			Pseudo-first-order model	
	Initial sorption rate (kq_e^2, min^{-1})	Equilibrium adsorption capacity (q_e, mg g^{-1})	R^2	Apparent photocatalytic degradation rate constant (k_{ap}, min^{-1})	R^2
4.0	1.93×10^{-1}	10.04	0.975	5.44×10^{-2}	0.953
6.8	7.60×10^{-2}	21.59	0.993	5.68×10^{-2}	0.984
10.0	4.97×10^{-2}	36.79	0.999	7.63×10^{-2}	0.847

Journal : Medium 11051 Dispatch : 12-9-2013 Pages : 13
Article No. : 1990 LE TYPESET
MS Code : NANO-D-13-01222 CP DISK

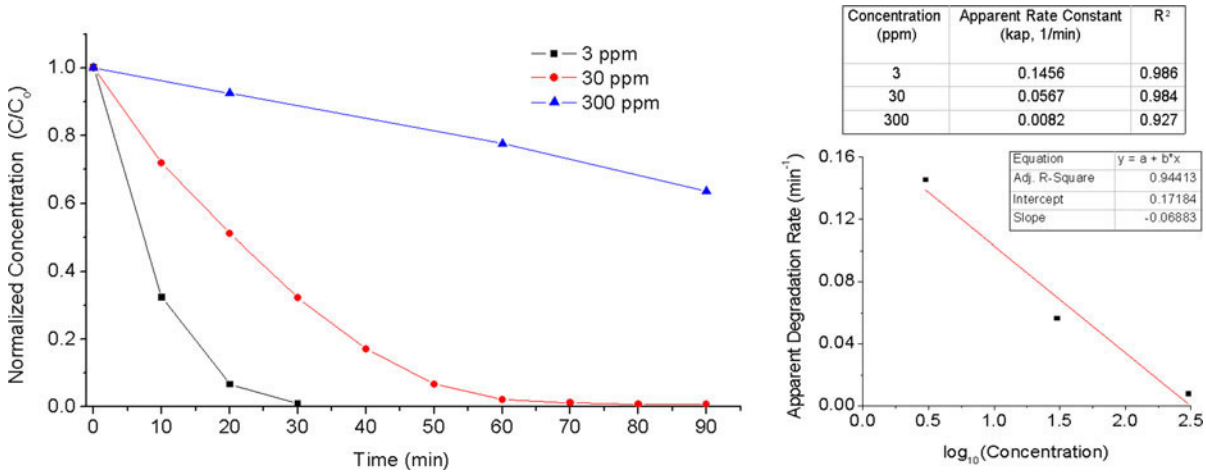

Fig. 10 Photocatalytic degradation of theophylline at concentrations of 3, 30, and 300 ppm

Concentration effects

The effect of pharmaceutical concentration on UV/TiO_2 photocatalytic degradation is evaluated in Fig. 10. At 3.0, 30, and 300 ppm the apparent degradation rates of theophylline were 1.46×10^{-1}, 5.67×10^{-2}, and 8.20×10^{-3} min^{-1}, respectively. For every magnitude increase in concentration of theophylline, the apparent degradation rate of theophylline would decrease at a rate of 0.0688 per ppm per min for concentrations from 3 to 300 ppm. At 30 min, the removal ratio of theophylline is 99, 68, and 11 % for an initial concentration of 3, 30, and 300 ppm, respectively. In addition, the total mass degraded over a span of 90 min was 15, 100, and 165 mg for an initial concentration of 3.0, 30, and 300 ppm. It seems that theophylline degradation reaches a saturation limit at high reactant concentrations.

Conclusions

Facile TiO_2 nanobelts for photocatalytic degradation of persistent pollutants in water treatment effluents were synthesized by autoclaving in concentrated alkaline NaOH solutions at 190 °C and annealing at 700 °C for 1 h. The TiO_2 nanobelt suspensions under UV illumination (peak wavelength: 365 nm) were able to degrade three select pharmaceuticals—carbamazepine, naproxen, and theophylline—through the generation of holes, hydroxyl radicals, and other oxidizing radical species. The experiments show that a high reaction temperature, an alkaline (high pH) solution, and concentration dependence favor faster photodegradation of theophylline. With the non-selectivity of hydroxyl radical generation from UV/TiO_2 nanobelt processes, even the most persistent organic compounds can be removed.

Acknowledgments This work has been financially supported by the Natural Sciences and Engineering Research Council of Canada through a strategic project grant, the Canadian Water Network Innovative Technologies for Water Treatment Program, and the Canada Research Chairs Program. Technical support from Trojan UV, the City of Guelph Wastewater Services, Deep Blue NRG, and GE Water & Process Technologies is highly appreciated.

References

Albu SP, Ghicov A, Macak JM, Hahn R, Schmuki P (2007) Self-organized, free-standing tio$_2$ nanotube membrane for flow-through photocatalytic applications. Nano Lett 7:1286–1289. doi:10.1021/nl070264k

Allen SJ, Mckay G, Khader KYH (1989) Intraparticle diffusion of a basic dye during adsorption onto sphagnum peat. Environ Poll 56:39–50. doi:10.1016/0269-7491(89)90120-6

Al-Qaradawi S, Salman SR (2004) Photocatalytic degradation of methyl orange as a model compound. J Photoche Photobiol A 148:161–168. doi:10.1016/S1010-6030(02)00086-2

Arrouvel C, Digne M, Breysse M, Toulhoat H, Raybaud P (2004) Effects of morphology on surface hydroxyl concentration: a DFT comparison of anatase-TiO_2 and γ-alumina catalytic supports. J Catal 222:152–166. doi:10.1016/j.jcat.2003.10.016

Journal : Medium 11051 Dispatch : 12-9-2013 Pages : 13
Article No. : 1990 LE TYPESET
MS Code : NANO-D-13-01222 CP DISK

Bahnemann D, Bockelmann D, Goslich R (1991) Mechanistic studies of water detoxification in illuminated TiO_2 suspensions. Solar Energy Mater 24:564–583. doi:10.1016/0165-1633(91)90091-X

Barka N, Qourzal S, Assabbane A, Nounah A, Ait-Ichou Y (2008) Factors influencing the photocatalytic degradation of Rhodamine B by TiO_2-coated non-woven paper. J Photochem Photobiol A 195(2–3):346–351. doi:10.1016/j.jphotochem.2007.10.022

Bloecher C (2007) Elimination of micropollutants and hazardous substances at the source in the chemical and pharmaceutical industry. Water Sci Technol 56(12):119–123. doi:10.2166/wst.2007.820

Bousselmi L, Geissen SU, Schroeder H (2004) Textile wastewater treatment and reuse by solar catalysis: results from a pilot plant in Tunisia. Water Sci Technol 49(4):331–337

Bouzaida I, Ferronato C, Chovelon JM, Rammah ME, Herrmann JM (2004) Heterogeneous photocatalytic degradation of the anthraquinonic dye, Acid Blue 25 (AB25): a kinetic approach. J Photochem Photobiol A 168:23–30. doi:10.1016/j.jphotochem.2004.05.008

Cho CH, Han MH, Kim DH, Kim DK (2005) Morphology evolution of anatase TiO_2 nanocrystals under a hydrothermal condition (pH = 9.5) and their ultra-high photocatalytic activity. Mater Chem Phys 92:104–111. doi:10.1016/j.matchemphys.2004.12.036

Fujishima A, Rao TN, Tyrk DA (2000) Titanium dioxide photocatalysis. J Photochem Photobio C 1(1):1–21. doi:10.1016/S1389-5567(00)00002-2

Giri RR, Ozaki H, Ota S, Takanami R, Taniguchi S (2010) Degradation of common pharmaceuticals and personal care products in mixed solutions by advanced oxidation techniques. Int J Environ Sci Tech 7(2):251–260

He J, Ma W, Song W, Zhao J, Qian X, Zhang S, Yu JC (2005) Photoreaction of aromatic compounds at αα-FeOOH/H_2O interface in the presence of H_2O_2: evidence for organic-goethite surface complex formation. Water Res 39(1):119–128. doi:10.1016/j.watres.2004.09.006

Henderson MA, Epling WS, Peden CHF, Perkins CL (2003) Insights into photoexcited electron scavenging processes on TiO_2 obtained from studies of the reaction of O_2 with oh groups adsorbed at electronic defects on TiO_2 (110). J Phys Chem B 107(2):534–545. doi:10.1021/jp0262113

Ho Y, McKey G (1998) The kinetics of sorption of basic dyes from aqueous solution by sphagnum moss peat. Can J Chem Eng 76(4):822–827. doi:10.1002/cjce.5450760419

Houas A, Lachheb H, Ksibi M, Elaloi E, Guillard C, Herrmann J (2001) Appl Catal B 31(2):145–157. doi:10.1016/S0926-3373(00)00276-9

Hu A, Zhang X, Oakes KD, Peng P, Zhou Y, Servos M (2011) Hydrothermal growth of TiO_2 nanowire membranes for ultrafiltration and photocatalytic degradation of pharmaceuticals. J Hazard Mater 189(1–2):278–285. doi:10.1016/j.jhazmat.2011.02.033

Hu A, Zhang X, Luong D, Oakes KD, Servos MR, Liang R, Kurdi S, Peng P, Zhou Y (2013) Adsorption and photocatalytic degradation kinetics of pharmaceuticals by TiO_2 nanowires during water treatment. Waste Biomass Valoriz 3:443–449. doi:10.1007/s12649-012-9142-6

Ishibashi K, Fujishima A, Watanabe T, Hashimoto K (2000) Quantum yields of active oxidative species formed on TiO_2 photocatalyst. J Photochem Photobiol A 134(1–2):139–142. doi:10.1016/S1010-6030(00)00264-1

Kim I, Tanaka H (2009) Photodegradation characteristics of PPCPs in water with UV treatment. Environ Int 25(5):793–802. doi:10.1016/j.envint.2009.01.003

Klavarioti M, Mantzavinos D, Kassinos D (2009) Removal of residual pharmaceuticals from aqueous systems by advanced oxidation processes. Environ Int 35(2):402–417. doi:10.1016/j.envint.2008.07.009

Kumar KV, Ramamurthi V, Sivanesan S (2005) Modeling the mechanism involved during the sorption of methylene blue onto fly ash. J Coll Int Sci 284:114–121. doi:10.1016/j.jcis.2004.09.063

Lapenna D, De Gioia S, Mezzetti A, Ciofani G, Festi D, Cuccurullo F (1995) Aminophylline: could it act as an antioxidant in vivo? Eur J Clin Invest 25(7):464–470

Li W, Liu C, Zhou YX, Bai Y, Feng X, Yang ZH, Lu LH, Lu XH, Chan KY (2008) Enhanced photocatalytic activity in anatase/TiO_2(B) core–shell nanofiber. J Phys Chem C 112(51):20539–20545. doi:10.1021/jp808183q

Li Q, Liu B, Wang L, Li D, Liu R, Zou B, Cui T, Zou G (2010) Pressure-induced amorphization and polyamorphism in one-dimensional single-crystal TiO_2 nanomaterials. J Phys Chem Lett 1(1):309–314. doi:10.1021/jz9001828

Lin H, Huang CP, Li W, Ni C, Ismat Shah S, Tseng Y (2006) Size dependency of nanocrystalline TiO_2 on its optical property and photocatalytic reactivity exemplified by 2-chlorophenol. Appl Catal B 68(1–2):1–11. doi:10.1016/j.apcatb.2006.07.018

Lin L, Chai Y, Zhao B, Wei W, He D, He B, Tang Q (2013) Photocatalytic oxidation for degradation of VOCs. Open J Inorg Chem 3:14–25. doi:10.4236/ojic.2013.31003

Malato S, Blanco J, Vidal A, Richter C (2002) Photocatalysis with solar energy at a pilot-plant scale: an overview. Appl Catal B 37(1):1–15. doi:10.1016/S0926-3373(01)00315-0

Malato S, Fernández-Ibáñez P, Maldonado MI, Blanco J, Gernjak W (2009) Decontamination and disinfection of water by solar photocatalysis: recent overview and trends. Catal Today 147(1):1–59. doi:10.1016/j.cattod.2009.06.018

Maoz A, Chefetz B (2010) Sorption of the pharmaceuticals carbamazepine and naproxen to dissolved organic matter: role of structural fractions. Water Res 44(3):981–989. doi:10.1016/j.watres.2009.10.019

Mazza T, Barborini E, Piseri P, Milani P, Cattaneo D, Li Bassi A, Bottani CE, Ducati C (2007) Raman spectroscopy characterization of TiO_2 rutile nanocrystals. Phys Rev B 75(4):045416-1-5. doi:10.1103/PhysRevB.75.045416

Mozia S, Tomaszewska M, Morawski AW (2007) Photocatalytic membrane reactor (PMR) coupling photocatalysis and membrane distillation—Effectiveness of removal of three azo dyes from water. Catal Today 129(1–2):3–8. doi:10.1016/j.cattod.2007.06.043

Naddeo V, Rizzo L, Belgiorno V (2011) Water, wastewater and soil treatment by advance oxidation processes. Lulu, Raleigh

Paola AD, Bellardita M, Palmisano L (2013) Brookite, the least known TiO_2 photocatalyst. Catalysts 3(1):36–73. doi:10.3390/catal3010036

Pignatello JJ, Oliveros E, Mackay A (2006) Advanced oxidation processes for organic contaminant destruction based on the fenton reaction and related chemistry. Crit Rev Environ Sci Technol 36(1):1–84. doi:10.1080/10643380500326564

Journal : Medium 11051 Dispatch : 12-9-2013 Pages : 13
Article No. : 1990 LE TYPESET
MS Code : NANO-D-13-01222 CP DISK

Quiroz MA, Bandala ER, Martinez-Huitle CA (2011) Advanced oxidation processes (AOPs) for removal of pesticides from aqueous media. In: Stoytcheva M (ed) Pesticides—formulations, Effects, Fate. InTech, Baltimore, pp 685–730

Rengifo-Herrera JA, Pizzio LR, Blanco MN, Roussel C, Pulgarin C (2011) Photocatalytic discoloration of aqueous malachite green solutions by UV-illuminated TiO_2 nanoparticles under air and nitrogen atmospheres: effects of counter-ions and pH. Photochem Photobiol Sci 10:29–34. doi:10.1039/C0PP00196A

Richardson SD (2008) Environmental mass spectrometry: emerging contaminants and current issues. Anal Chem 80:4373–4402. doi:10.1021/ac800660d

Richardson SD, Thurston AD, Collette TW, Patterson KS, Lykins BW, Ireland JC (1996) Identification of TiO_2/UV disinfection byproducts in drinking water. Environ Sci Technol 30:3327–3334. doi:S0013-936X(96)00142-3

Rizzo L, Meric S, Guida M, Kassinos D, Belgiorno V (2009) Heterogeneous photocatalytic degradation kinetics and detoxification of an urban wastewater treatment plant effluent contaminated with pharmaceuticals. Water Res 43(16):4070–4078. doi:10.1016/j.watres.2009.06.046

Rosal R, Rodriguez A, Perdigon-Melon JA, Petre A, Garcia-Calvo E, Gomez MJ, Aguera A, Fernandez-Alba AR (2010) Occurrence of emerging pollutants in urban wastewater and their removal through biological treatment followed by ozonation. Water Res 44(2):578–588. doi:10.1016/j.watres.2009.07.004

Selcuk H (2010) Disinfection and formation of disinfection by-products in a photoelectrocatalytic system. Water Res 44(13):3966–3972. doi:10.1016/j.watres.2010.04.034

Sikuvhihulu LC, Coville NJ, Ntho T, Scurrell MS (2008) Potassium titanate: an alternative support for gold catalyzed carbon monoxide oxidation. Catal Lett 123(3–4): 193–197. doi:10.1007/s10562-008-9439-z

Sirés I, Brillas E (2012) Remediation of water pollution caused by pharmaceutical residues based on electrochemical separation and degradation technologies: a review. Environ Int 40:212–229. doi:10.1016/j.envint.2011.07.012

Solarchem Environmental Systems (1994) The UV/oxidation handbook. Solarchem Environmental Systems, Markham

Sua′ rez S, Carballa M, Omil F, Lema JM (2008) How are pharmaceutical and personal care products (PPCPs) removed from urban wastewaters? Rev Environ Sci Biotechnol 7:125–138. doi:10.1007/s11157-008-9130-2

Sun Q, Yang L (2003) The adsorption of basic dyes from aqueous solution on modified peat–resin particle. Water Res 37(7):1535–1544. doi:10.1016/S0043-1354(02)00520-1

Tauc J, Grigorovici R, Vancu A (1966) Optical properties and electronic structure of amorphous germanium. Phys Stat Sol 15:627–637. doi:0.1002/pssb.19660150224

Walker GM, Hansen L, Hanna JA, Allen SJ (2003) Kinetics of a reactive dye adsorption onto dolomitic sorbents. Water Res 37(9):2081–2089. doi:10.1016/S0043-1354(02)00540-7

Weber WJ, Morriss JC (1963) Kinetics of adsorption of carbon from solution. J Sanit Eng Div Am Soc Civ Eng 89:31–51

Wintgens T, Salehi F, Hochstrat R, Melin T (2008) Emerging contaminants and treatment options in water recycling for indirect potable use. Water Sci Technol 57(1):99–107. doi:10.2166/wst.2008.799

Wu Z, Dong F, Zhao W, Wang H, Liu Y, Guan B (2009) The fabrication and characterization of novel carbon doped TiO_2 nanotubes, nanowires and nanorods with high visible light photocatalytic activity. Nanotechnology 20:235701. doi:10.1088/0957-4484/20/23/235701

Wu W, Lei B, Rao H, Xu Y, Wang Y, Su C, Kuang D (2013) Hierarchical oriented anatase TiO_2 nanostructure arrays on flexible substrate for efficient dye-sensitized solar cells. Sci Rep 3:1352. doi:10.1038/srep01892

Yang D, Liu H, Zheng Z, Yuan Y, Zhao J, Waclawik ER, Ke X, Zhu H (2009) An efficient photocatalyst structure, TiO_2(B) nanofibers with a shell of anatase nanocrystal. J Am Chem Soc 131:17885–17893. doi:10.1021/ja906774k

Yao WF, Xu XH, Wang H, Zhou JT, Yang XN, Zhang Y, Shang SX, Huang BB (2004) Photocatalytic property of perovskite bismuth titanate. Appl Catal B 52(2):109–116. doi:10.1016/j.apcatb.2004.04.002

Yin S, Uchida S, Fujishiro Y, Wu J, Aki M, Sato T (2000) Photocatalytic properties of titania prepared by the solvothermal reactions of protonic layered tetratitanate. Int J Inorg Mater 2:325–331

Zárate RA, Fuentes S, Wiff JP, Fuenzalida VM, Cabrera AL (2007) Chemical composition and phase identification of sodium titanate nanostructures grown from titania by hydrothermal processing. J Phys Chem Solids 68(4): 628–637. doi:10.1016/j.jpcs.2007.02.011

Zhang X, Sun DD, Li G, Wang Y (2008) Investigation of the roles of active oxygen species in photodegradation of azo dye AO7 in TiO_2 photocatalysis illuminated by microwave electrodeless lamp. J Photochem Photobiol A 199(2–3): 311–315. doi:10.1016/j.jphotochem.2008.06.009

Zhang X, Pan J, Du A, Fu W, Sun D, Leckie J (2009) Combination of one-dimensional TiO_2 nanowire photocatalytic oxidation with microfiltration for water treatment. Water Res 43:1179–1186. doi:10.1016/j.watres.2008.12.021

Zheng Z, Liu H, Ye J, Zhao J, Waclawik ER, Zhu H (2010) Structure and contribution to photocatalytic activity of the interfaces in nanofibers with mixed anatase and TiO_2(B) phases. J Mol Catal A 316:75–82. doi:10.1016/j.molcata.2009.10.002

Zhou W, Liu H, Wang J, Liu D, Du G, Han S, Lin J, Wang R (2010) Interface dominated high photocatalytic properties of electrostatic self-assembled Ag_2O/TiO_2 heterostructure. Phys Chem Chem Phys 12:15119–15123. doi:10.1039/C0CP00734J

Journal : Medium 11051 Dispatch : 12-9-2013 Pages : 13
Article No. : 1990 ☐ LE ☐ TYPESET
MS Code : NANO-D-13-01222 ✔ CP ✔ DISK

Journal : **11051**
Article : **1990**

Springer
the language of science

Author Query Form

Please ensure you fill out your response to the queries raised below and return this form along with your corrections

Dear Author

During the process of typesetting your article, the following queries have arisen. Please check your typeset proof carefully against the queries listed below and mark the necessary changes either directly on the proof/online grid or in the 'Author's response' area provided below

Query	Details Required	Author's Response
AQ1	Please note that the equations are renumbered to ensure sequential ordering.	